European Rotorcraft Forum

EXPERIMENTAL AND NUMERICAL STUDY OF PARALLEL BLADE-VORTEX INTERACTION

Andrea Colli*, Antonella Abbà, Giuseppe Gibertini
Politecnico di Milano, Milano - Italy
* andrea.colli@polimi.it

Abstract

Parallel Blade-Vortex Interaction is studied both via experimental wind-tunnel tests with wing models in a tandem setup and via LES simulations. A *p*-adaptive Local Discontinuous Galerkin approach is used, with a physically based refinement indicator and a dynamic anisotropic eddy viscosity model for subgrid scale turbulent stresses. The results validate the numerical tool and show its efficacy and efficiency in the simulation of BVI, succesfully extending the range of investigation of the experimental setup.

List of symbols

U_∞	free-stream speed
c	blade model chord
c_g	vortex generator chord
u	horizontal velocity component
α_geo	blade model geometric angle of incidence
α_eq	blade model equivalent angle of incidence
α_g	vortex generator angle of incidence
u_θ	vortex tangential velocity
r	vortex core radius
R_v	ratio of vortex core radius over blade model chord
Γ	circulation around vortex core perimeter
t	non-dimensional time
$\mathbf{U}$	vector of filtered variables
ρ	density
e	total energy per unit volume
$\mathbf{u}$	velocity vector
T	temperature
τ_{ij}^sgs	subgrid stress tensor
$\mathbf{Q}^\mathrm{sgs}$	subgrid heat flux
$\mathbf{J}^\mathrm{sgs}$	subgrid turbulent diffusion flux
$\bar{\cdot}$	space filter operator
$\widetilde{\cdot}$	Favre filter operator
D_{ij}	structure function
D_{ij}^iso	structure function in isotropic conditions
Ind_SF	structure function indicator
(x_v, y_v)	vortex initial coordinates

1 INTRODUCTION

Blade-vortex interaction (BVI), is an important aerodynamic phenomenon for all kinds of rotary-wing aircraft, ranging from helicopters to more complex eVTOL configurations and also to drones and other Micro Aerial Veichles (MAVs). The study of BVI is therefore of interest, in particular since it has been shown [1, 2, 3, 4, 5] that this interaction can have a direct effect on the loads generated by a rotor and also trigger dynamic stall. While this was observed for the specific case of perpendicular BVI, this work analyzes the case of parallel BVI, to investigate if similar effects can occour and evaluate their severity. Stemming from previous related studies [6, 7], the approach followed in this work is twofold, combining both experimental wind-tunnel measurements of parallel blade-vortex interaction and numerical Large Eddy Simulation (LES) of the same test case: this allows for a direct comparison of the results, which, to the authors' knowledge, is not yet available in literature for this kind of analysis. The benefits of such a comparison are not only the validation of the numerical tool with the data from the measurements, but also the subsequent possibility of using this tool to investigate conditions not easily reproduced by experiment.

2 EXPERIMENTAL INVESTIGATION

Following the steps of a previous study [6], a wind-tunnel test campaign is undertaken to investigate the parallel interaction between an airfoil and a singular vortex and to obtain data for further comparison with numerical simulations. The experimental setup is composed of two airfoil models in a tandem configuration (Figure 1), namely the vortex generator, placed upstream, and the blade model, downstream of the generator. The vortex generator has a custom hybrid NACA 0018/ NACA 0025 airfoil section and a chord of $c_g = 0.2\,\mathrm{m}$, while the blade model has the NACA 23012 airfoil section and a chord of $c = 0.3\,\mathrm{m}$; both models have a span of $0.96\,\mathrm{m}$. The generation of the vortex was obtained by impulsively pitching the vortex generator by means of an electrical motor connected to it. The rotation, about the airfoil quarter-chord, was performed from a geometric angle of incidence of $\alpha_g = 0°$ to $\alpha_g = 10°$ in about

Presented at the 48th European Rotorcraft Forum, Winterthur, Switzerland, 6-8 September, 2022

$11\,\mathrm{ms}$. The tests were conducted in the "S. De Ponte" low-speed, closed-return wind tunnel at Politecnico di Milano, which has a rectangular test section $1.5\,\mathrm{m}$ high and $1\,\mathrm{m}$ wide and a maximum wind speed of $55\,\mathrm{m/s}$. For the experiments the free-stream speed was $U_\infty = 15\,\mathrm{m/s}$, corresponding to a Reynolds number based on the blade model chord of $300\,000$, chosen in relation to the execution time of the generator's pitching motion. The vortex generation and the subsequent interaction with the blade model were measured with Particle Image Velocimetry (PIV) techniques, in order to study the flow field in the region around the airfoil. Pressure measurements were also performed, both steady and unsteady, to evaluate the loads on the airfoil and their variation due to the interaction. Different configurations, in terms of relative position between the vortex generator and the blade model, were examined. Given the tandem setup, particular care was needed in treating the interference effect of the vortex generator, especially in view of the comparison with the numerical simulations. To this end, a computation of the relative corrections and a measure of the turbulence level via hot-wire anemometry are performed.

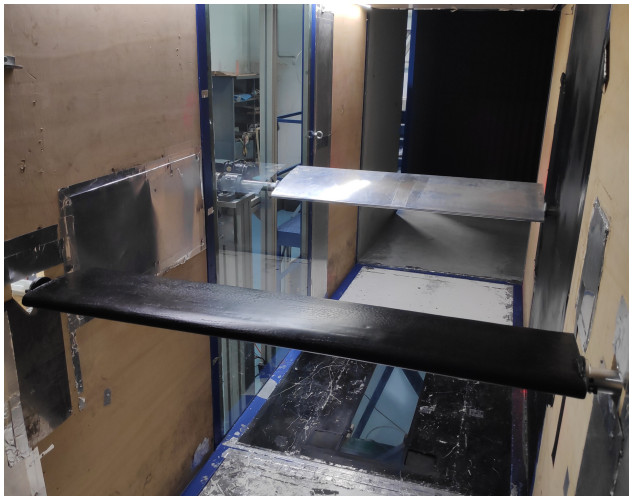

Figure 1: Test rig setup in the wind tunnel. The vortex generator is visible in the foreground, while the blade model is in the background.

2.1 PIV measurements

Particle Image Velocimetry was chosen as the main tool for the study of BVI because it allows to readily obtain measurements of whole regions of the flow field, from which to extract information on the generated vortex, its trajectory and the effects on the flow around the airfoil. This is fundamental especially in setting up the test rig, ensuring that the position of the vortex generator relative to the airfoil and its pitching motion are adequate for the desired kind of interaction. For this reason, three main typologies of data acquisition are performed: the first one is devoted to the characterization of the generated vortex, which is measured in the empty (i.e. without the airfoil model) test section of the wind tunnel in order to assess its circulation and shape; secondly, the airfoil model is inserted in the test section and measurements are made of the flow field in the region immediately upstream of it, at different time instants, with the purpose of tracking the vortex trajectory with respect to the airfoil and consequently of adjusting the vertical position of the vortex generator, if needed; finally, the interaction of the vortex with the flow around the airfoil is studied by measuring the flow field in the region over the airfoil's suction side at different time instants, thus effectively investigating the event sequence.

The PIV setup was composed of a dual Nd-YAG Evergreen laser, with an energy of $200\,\mathrm{mJ}$ per pulse and placed below an optic window in the midspan of the test section floor, to illuminate the flow field, while images was acquired by a couple of iLA5150 sCMOS cameras, with a resolution of $2560\mathrm{x}2160$ pixel. Subsequent processing of the images was performed via the PivTec PivView2C software: correlation was performed with a multi-pass method over a $32\mathrm{x}32$ pixel grid and finally a phase average was computed from the resulting data. The timing of the acquisition was controlled by means of an iLA5150 Synchronizer, with the sequence triggered by a Hall effect magnetic sensor installed on the vortex generator support structure, such as to emit a signal when the vortex generator would pass a determined angular position in its pitching motion; a time delay was then added and adjusted to obtain measures at different instants as required. Each single acquisition is composed of a series of 200 couples of images. As a reference for the uncertainty of the PIV measurements, a value of 0.1 pixel is taken, corresponding to $0.13\,\mathrm{mm}$.

2.2 PIV results

Figure 2 shows the vorticity contour computed from PIV data for the vortex characterization phase. The vortex has a circular shape, with a core radius, defined as the distance from the centre at which the tangential velocity u_θ is maximum, of $12.7\,\mathrm{mm}$, while the maximum tangential velocity itself is of $4.25\,\mathrm{m/s}$; the computed circulation around the core perimeter is $0.331\,\mathrm{m^2/s}$. The test rig gave fully satisfactory results for what concerns vortex generation, producing a well-defined, isolated vortex with good repeatability: the root mean square of the vortex centre position, considering all 200 couples of images, was $3.1\,\mathrm{mm}$. However, comparison with data from experimental measurements of a rotor tip vortex [8] shows that the strength of such a vortex is around three times that of the vortex generated by the current setup, while the dimension is comparable. This defect of the experimental tests is addressed and overcome in the numerical simulations described below (section 3).

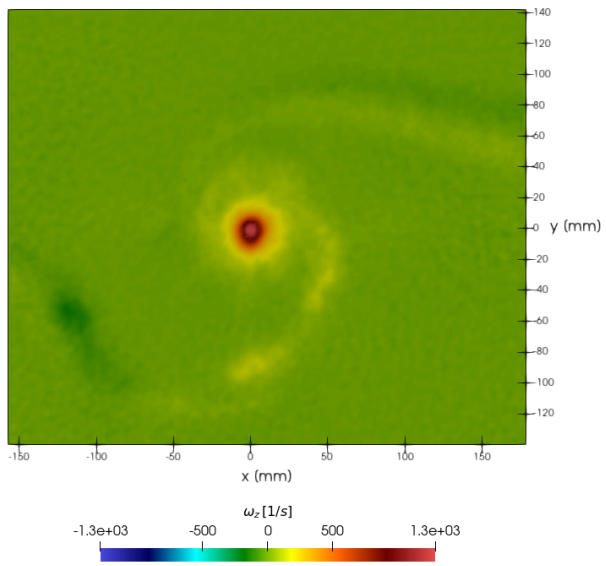

Figure 2: Vorticity contour from PIV measurement of the isolated vortex.

In Figure 3 results are presented of the PIV measurement of the flow region immediately upstream of the blade model, showing the trajectory of the approaching vortex. It can be noticed how the vorticity peak gets progressively lower as the vortex interacts with the flow around the airfoil.

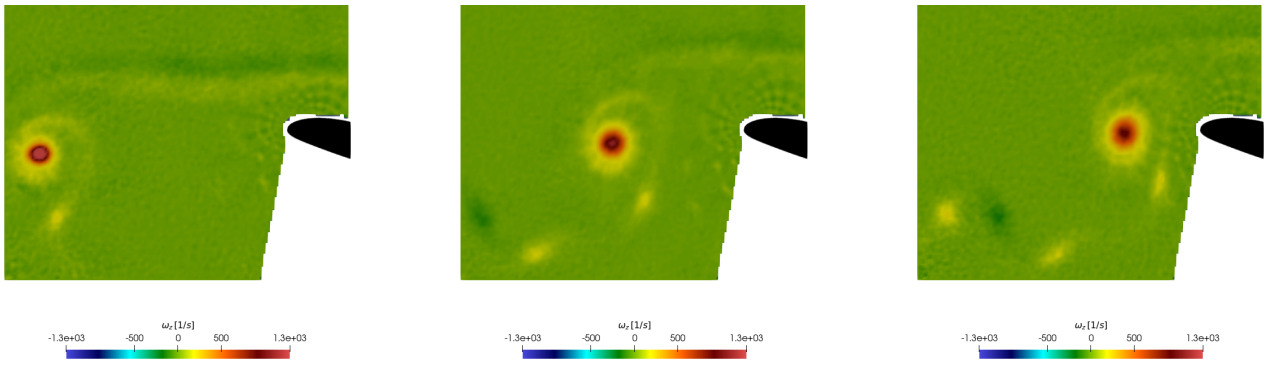

(a) $t = 2.5$ (b) $t = 2.9$ (c) $t = 3.1$

Figure 3: Vorticity contour from PIV measurement of the vortex approaching the blade model. Time instants t are non-dimensional for ease of reference with the LES results presented in section 3.

Results from the PIV measurements over the full airfoil suction side are shown in Figure 4 in terms of contours of the horizontal component u of the velocity. Figure 4a represents the flow condition when no BVI is occurring, i.e. without any vortex having been generated, and is therefore the reference condition. Figure 4b and onward show instead the effects of the interaction with the vortex: as the vortex approaches, a region of separated flow can be seen forming near the trailing edge of the airfoil and with the vortex passing over the airfoil this region extends slightly upstream at first, then reduces back to the trailing edge region as the vortex moves past the airfoil; the return to conditions comparable to those with no interaction occurs only after the vortex has further traveled about $1.5c$ downstream of the leading edge (Figure 4g). The corresponding results in terms of the vorticity field can be found below in Figure 15.

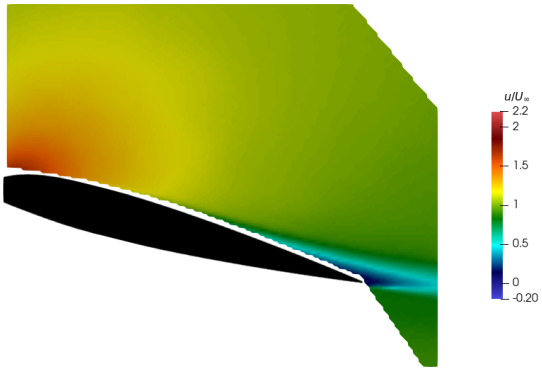

(a) No BVI

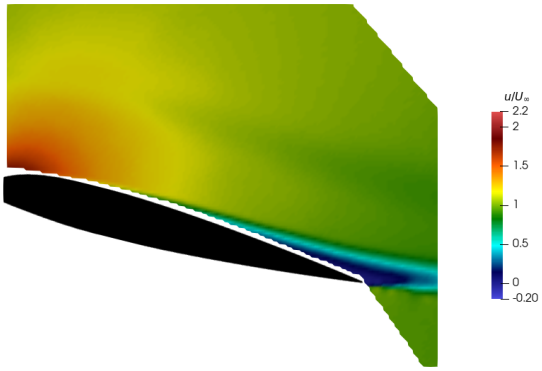

(b) $t = 3.1$

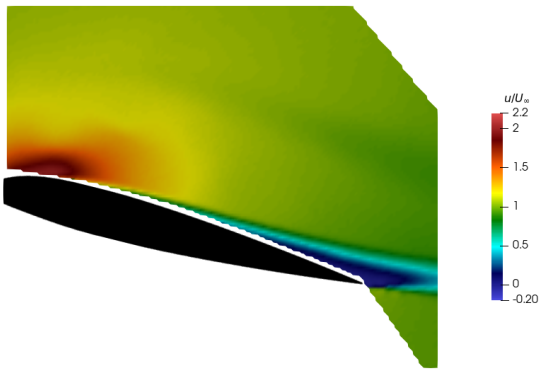

(c) $t = 3.5$

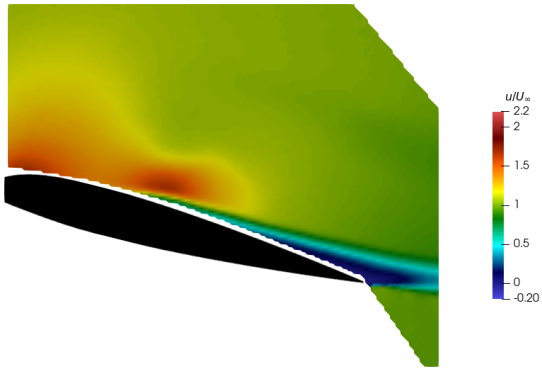

(d) $t = 3.7$

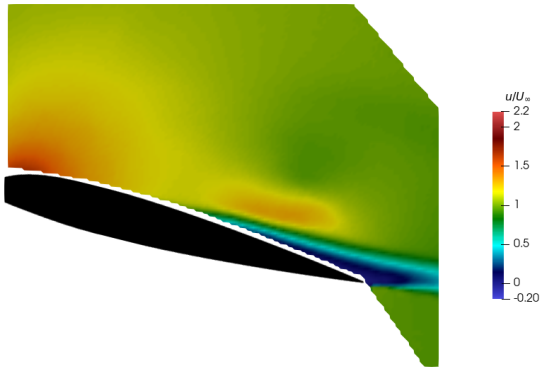

(e) $t = 4$

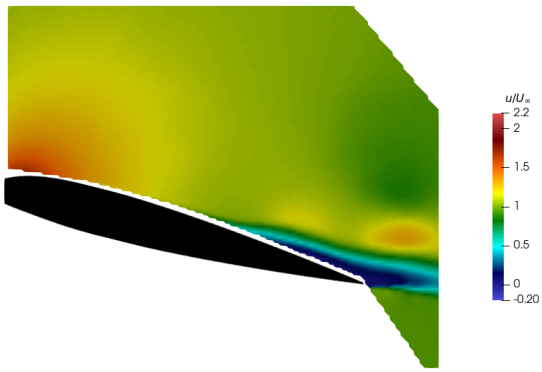

(f) $t = 4.2$

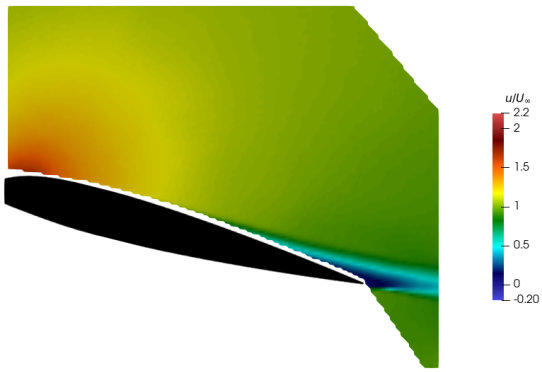

(g) $t = 5.6$

Figure 4: Contours of the horizontal component u of the velocity from PIV measurements of the flow field in the region around the suction side of the blade model, with no vortex interaction occurring (a), and at different time instants during blade-vortex interaction (b-g). Time instants t are non-dimensional for ease of reference with the LES results presented in section 3.

2.3 Pressure measurements

In order to evaluate the effect of the blade-vortex interaction on the aerodynamic loads of the airfoil, pressure measurements were performed. The blade model structure allows for the installation of two interchangeable mid-sections, one used for PIV measurements and one used for pressure measurements; the latter is equipped with 21 pressure taps distributed along the chord (Figure 5).

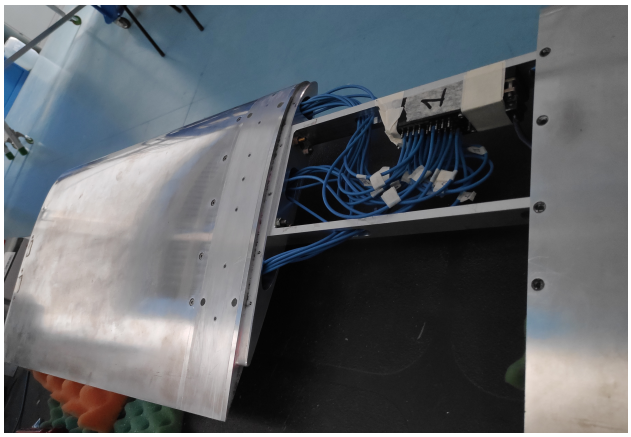

Figure 5: Detail of the blade model with a lateral section removed to show the pressure scanner and the tubes connecting to the pressure taps in the middle section.

Steady pressure measurements were performed by means of a PSI miniature pressure scanner. These measurements were then integrated to compute the lift coefficient on the blade model at different angles of attack, both in an isolated configuration, i.e. without the vortex generator in the wind tunnel test section, and with the generator installed at different incidence angles (Figure 6). This data was used to evaluate the interference effect of the generator and in general to determine the wind-tunnel corrections, which are then used to set up the numerical simulation.

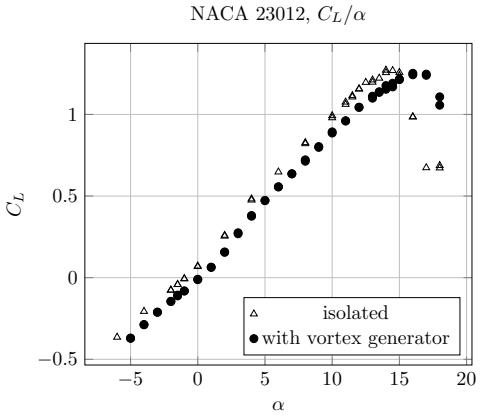

Figure 6: Lift coefficient variation with geometric incidence for the isolated NACA 23012 blade model and with the vortex generator installed in the wind tunnel with an incidence of $\alpha_g = 10°$.

3 NUMERICAL SIMULATION

3.1 LES numerical method

Following previous works in literature [7, 9], a numerical code implementing a Local Discontinuous Galerkin (LDG) finite element (FE) method was used for the LES computation, together with the anisotropic subgrid scale (sgs) model developed in [10]. More details on the specific code implementation, which is based on the `FEMilaro` library, are available in [11]. With this approach, the filtered compressible Navier-Stokes equations,

$$\partial_t \mathbf{U} + \nabla \cdot \mathbf{F}(\mathbf{U}) = 0 \tag{1}$$

are discretized in space and reduced to the first order system

$$\begin{aligned} \partial_t \mathbf{U} + \nabla \cdot \mathbf{F}(\mathbf{U}, \mathbf{G}) &= 0 \\ \mathbf{G} - \nabla \phi &= 0, \end{aligned} \tag{2}$$

where $\mathbf{U} = [\overline{\rho}, \widetilde{\overline{\rho}\mathbf{u}}^T, \widetilde{\overline{\rho e}}]^T$ is composed of the filtered variables, namely the density, momentum and total energy per unit volume, $\bar{\cdot}$ and $\tilde{\cdot}$ are, respectively, the space filter and the Favre filter operators, $\mathbf{F}$ is the flux, containing the convective flux, the viscous flux and the modeled subgrid flux, $\mathbf{G}$ is an auxiliary variable and $\phi = [\widetilde{\mathbf{u}}^T, \widetilde{T}]^T$ contains the filtered temperature $\widetilde{T}$.

In particular, this model is characterised by the anisotropic subgrid flux

$$\mathbf{F}^{\text{sgs}} = \begin{bmatrix} 0 \\ \tau^{\text{sgs}} \\ \frac{1}{k}\mathbf{Q}^{\text{sgs}} + \frac{\gamma \text{Ma}^2}{2}\left(J - \tau^{\text{sgs}}_{kk}\tilde{\boldsymbol{u}}\right) \end{bmatrix}, \tag{3}$$

where τ^{sgs}_{ij} is the sgs stress tensor, $\mathbf{Q}^{\text{sgs}}$ the sgs heat flux and $\mathbf{J}^{\text{sgs}}$ the sgs turbulent diffusion flux.

The numerical domain is tessellated with tetrahedral elements, over which a discontinuous finite element space of polynomial functions is defined. The polynomial degree can vary both in space and time for each element, adapting to a local resolution requirement. The metric for the choice of the degree is based on a structure function sensitive to the local conditions of the turbulent flow,

$$\text{Ind}_{\text{SF}}(K) = \sqrt{\sum_{ij}\left(D_{ij} - D^{\text{iso}}_{ij}\right)^2}, \tag{4}$$

where Ind_{SF} is the structure function indicator, D_{ij} is the structure function, defined by

$$D_{ij} = \langle [u_i(\mathbf{x}+\mathbf{r},t) - u_i(\mathbf{x},t)]\,[u_j(\mathbf{x}+\mathbf{r},t) - u_j(\mathbf{x},t)] \rangle \tag{5}$$

and D^{iso}_{ij} is the structure function in isotropic conditions. More details are available in [12]. Finally, the advancement in time of the discretized equations is performed by employing the explicit five-stages fourth-order Strong Stability Preserving Runge-Kutta method.

3.2 Simulation setup

This numerical code was applied to the simulation of the wind-tunnel experiments, namely the parallel interaction between a vortex and an infinite wing with the NACA 23012 airfoil section at a chord-based Reynolds number $Re = \frac{\rho_\infty U_\infty}{\mu_\infty} = 300\,000$ and at Mach number $Ma = \frac{U_\infty}{a_\infty} = 0.1$. In the following, dimensionless quantities are understood unless otherwise specified, using the airfoil chord $C = 0.3\,\mathrm{m}$ and the free-stream speed $U_\infty = 15\,\mathrm{m/s}$ as reference length and speed, respectively.

Particular care was required to determine the angle of incidence of the wing in order to reproduce flow conditions equivalent to those found in the wind-tunnel tests. Instead of relying on empiric relations for the various corrections to be applied, an approach based on the knowledge of the pressure distribution over the airfoil was used. To this end, a preliminary computation of the NACA 23012 airfoil at different incidences was done using the XFOIL software and a condition α_{eq} was found for which the pressure distribution closely matches the one measured in the wind tunnel for the geometrical incidence $\alpha_{\text{geo}} = 14\,°$ at which the tests were performed. This agreement was then confirmed by checking against the results of the LES simulation of the developed flow around the wing, before continuing with the computation of the vortex interaction. With this procedure, an equivalent incidence $\alpha_{\text{eq}} = 10\,°$ was determined.

Around the airfoil the computational domain is discretized adopting the grid shown in Figure 7, with inflow, upper and lower boundaries positioned 5 units from the leading edge, while the outflow boundary is 10 units downstream of the airfoil; the mesh is extruded 0.2 units in the spanwise direction. The grid is composed of $299\,756$ tetrahedra. Far-field conditions are imposed at the inflow, sponge layers are applied on the outflow, upper and lower boundaries, cyclic conditions are imposed in the spanwise direction, while on the airfoil itself the no-slip isothermal boundary condition is applied. A refinement line is introduced upstream of the airfoil, to avoid excessive dissipation of the vortex which is introduced to simulate the interaction.

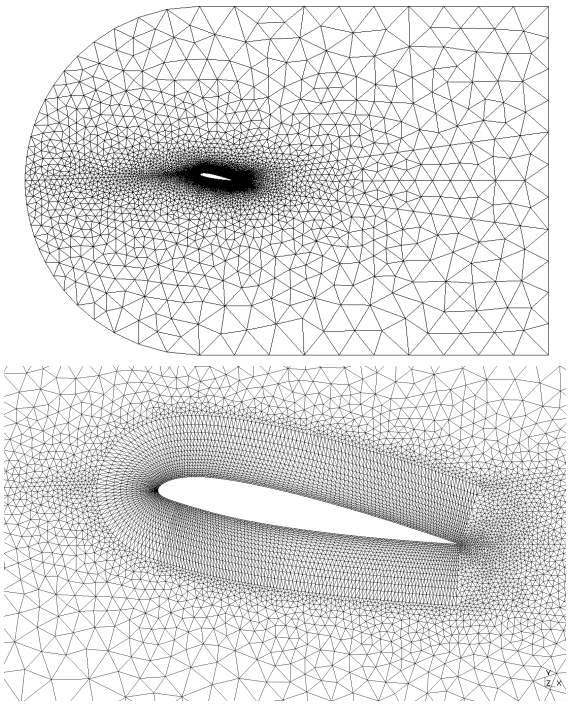

Figure 7: Two-dimensional representation of the full computational grid (top) and closer view on the structured region around the airfoil (bottom)

For the simulations, the maximum polynomial degree is allowed to vary between 2 and 4, with 3 selected for values of the local indicator intermediate between two thresholds. In the adaptive process, only changes of at most one degree, either increasing or decreasing, are allowed, and the computational load is redistributed as needed using `mpmetis` to avoid unbalances between processors in a parallel run.

3.3 LES computations

Firstly, the developed flow around the wing in the absence of the vortex was computed, both to provide a reference for the comparison with the interaction case and to verify the agreement with the experimental data in this configuration.

Next, the vortex is introduced in this developed flow upstream of the airfoil and its convection and subsequent interaction with the airfoil itself is computed. To model the vortex, the Vatistas' formulation [13]

$$u_\theta = \frac{r}{(1 + r^{2n})^{\frac{1}{n}}} \tag{6}$$

with $n = 1$ is chosen (essentially reducing to Rosenhead's model[14]), which gives a tangential velocity distribution in good agreement with the one measured for the experimental vortex as seen in Figure 8. The physical parameters are chosen in order to best reproduce the conditions of the wind-tunnel tests: the counter-clockwise vortex has axis parallel to the wing span direction and a radius of $R_v = 0.0423$; for the initial position (x_v, y_v) of the vortex, two cases were considered:

- case A $(x_v, y_v) = (-3.3, -0.015)$;
- case B $(x_v, y_v) = (-3.3, -0.0166)$;

the former corresponding to a vortex trajectory passing above the airfoil, while the latter corresponds to a trajectory impinging on the leading edge. Concerning the vortex circulation, finally, two conditions were tested: the first with a circulation equal to that of the experimental vortex, to be able to compare and validate the results with wind tunnel data; the second with a circulation around three times higher, in order to simulate an interaction with a vortex more similar to a rotor's tip vortex and therefore overcome the limitations of the experimental setup, as described above.

The computations were run on the High Performance Computing system "Betzy", a BullSequana XH2000 supercomputer located at NTNU in Trondheim, with 2048 AMD® EPYC™ 7742 CPUs. With a timestep of 1×10^{-5} and a final time of 6, the time required for a simulation of blade-vortex interaction was about 24 hours.

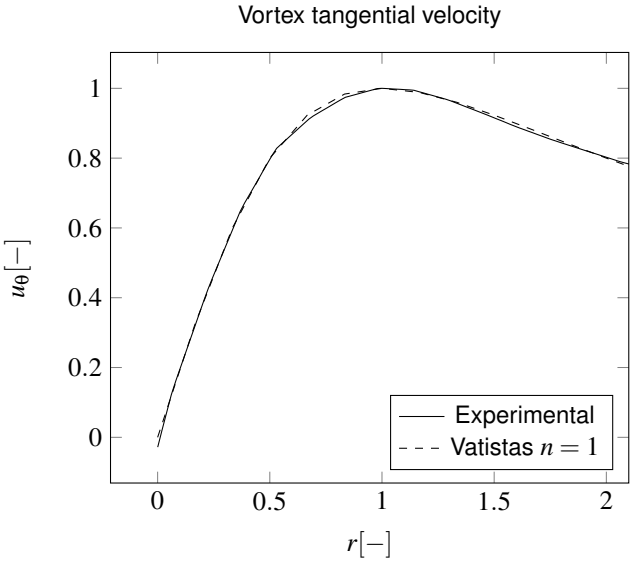

Figure 8: Comparison between the experimental vortex tangential velocity and Vatistas analytical model with $n = 1$; the tangential velocity and the vortex radius have been normalized with the maximum velocity and the core radius, respectively.

4 SIMULATION RESULTS

4.1 Developed flow

For the computation of the developed flow a static adaptivity approach was chosen for the polynomial degree, resulting in a total of 3.7×10^6 degrees of freedom; in Figure 9 the distribution of the polynomial degree in the computational domain can be seen, showing how the higher degrees are employed for the boundary layer and near wake of the airfoil.

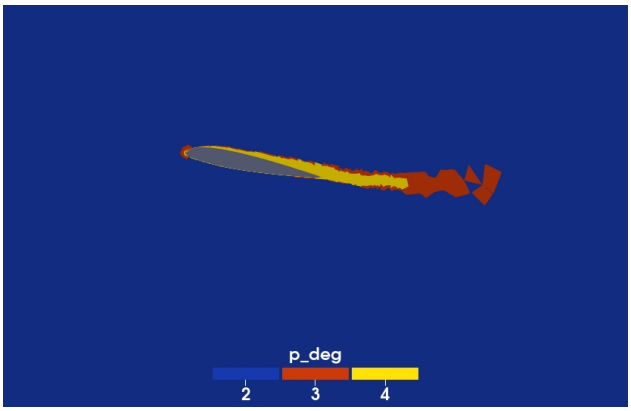

Figure 9: Polynomial degree distribution of the finite element functions in the computational domain for the developed flow computation.

A comparison of the pressure coefficient distribution around the NACA 23012 wing obtained by the LES computation with that measured in the wind tunnel is presented in Figure 10: the agreement is rather good, confirming the evaluation of the equivalent incidence. However, the presence of a laminar separation bubble can be evinced which does not appear from the experimental data.

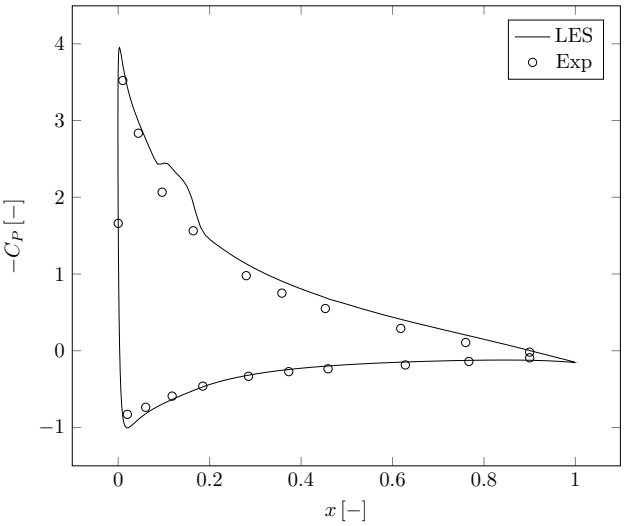

Figure 10: Chord-wise pressure coefficient distribution on the wing.

In terms of aerodynamic coefficients, the following results were obtained for lift, drag, and pitching moment:

$$(7) \quad C_L = 1.203 \qquad C_D = 0.02015 \qquad C_M = -0.000379$$

Figure 11 shows the contour of the horizontal component of the velocity field.

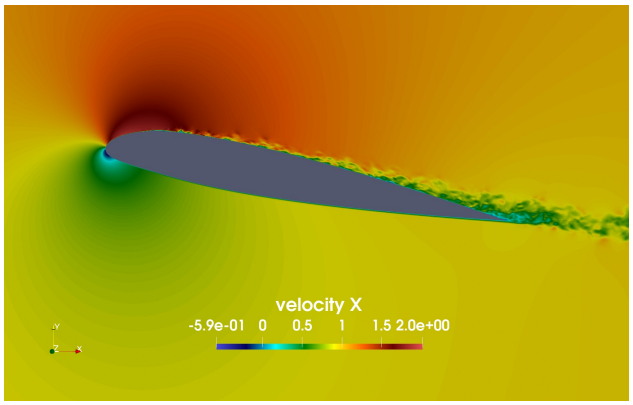

Figure 11: Horizontal component of the velocity field.

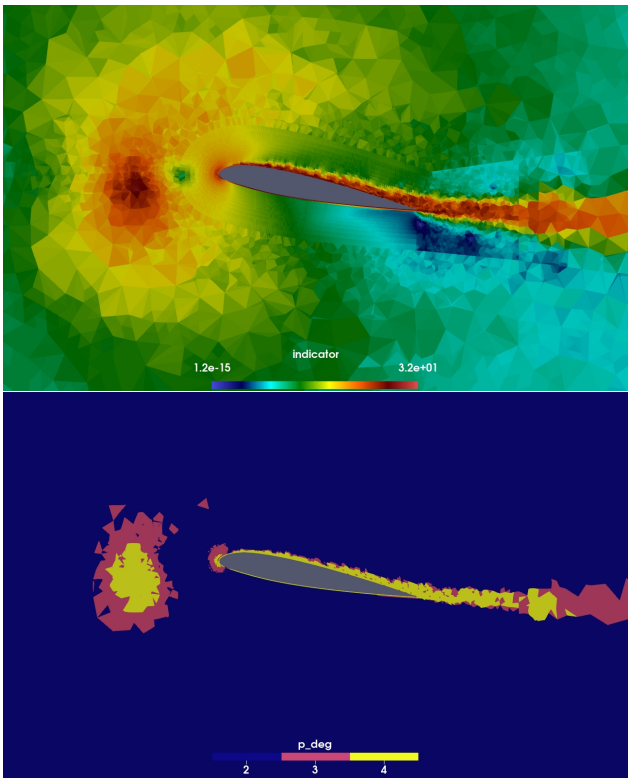

Figure 12: Indicator value (top) and polynomial degree distribution (bottom) for the vortex interaction in case A, $t = 3$. The vortex can be seen immediately upstream of the airfoil. See also Figure 3b and Figure 3c for comparison with the experimental data.

4.2 Vortex interaction

For the computation of the blade-vortex interaction a dynamic approach to the polynomial adaptivity was employed by updating the polynomial degree every 30 time steps, based on a time average, over the same interval, of the indicator value. An example of the distribution of the indicator value and of the resulting degree of the finite element functions is shown in Figure 12, representing the approach of the vortex in case A: comparing it with Figure 9, the effectiveness of the adaptive approach and of the choice of indicator can be seen as the area of the vortex is correctly identified and the higher degrees employed to compute the solution there. The maximum number of degrees of freedom during the computation of the vortex interaction is 4.0×10^6, which is less than $37\,\%$ of the degrees of freedom to be used for uniform P^4 polynomials.

The results from the simulation with the vortex circulation equal to that of the experimental vortex and those with the increased circulation are qualitatively similar and in the following only the latter are presented. In general, they show an interaction process which agrees with that evidenced by the experimental PIV data. However, no significant separation of the flow is apparent, or, if present, only in a very small region. An example of the velocity field around the airfoil is shown in Figure 13, to be compared to the experimental results in Figure 4.

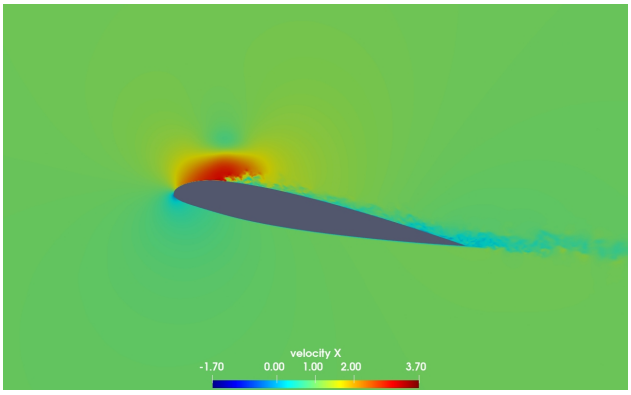

Figure 13: Contour of the horizontal component u of the velocity field from LES computation at $t = 3.5$

The time history of the lift, drag and pitching moment coefficients can be seen in Figure 14 and by analysing it also in relation to Figure 15, which shows the vorticity contours at different time instants, the details of the blade-vortex interaction can be studied. Firstly, it can be noticed how the behaviour is qualitatively very similar between the cases A and B, with a slightly higher excursion of the coefficients for the case of the vortex directly impinging on the leading edge of the wing. Secondly, as expected of BVI, the aerodynamic loads exhibit a relevant variation with respect to their values when no interaction occurs; this variation is more evident as the vortex approaches and has a sharp peak as the vortex passes above the leading edge region (for $t = 3.4$ and $t = 3.5$, see Figure 15a and Figure 15b). While the lift coefficient experiences an increase of $81\,\%$, up to a maximum of 2.183, it is interesting how the drag coefficient decreases by over sixteen times its value in the reference case with no interaction, becoming negative, $C_D = -0.32$. The pitching moment coefficient also shows a drastic diminishing to values as low as -0.24. This variations in the forces on the wing can be explained by the pressure drop accompanying the counter-clockwise vortex: as this low pressure structure sweeps over the leading edge of the airfoil it results in an increase of lift and the drop is strong enough that the difference with the pressure on the back of the airfoil produces the negative drag observed. As the vortex is further convected downstream, it starts to interact with the airfoil boundary layer (Figure 15c to 15f) the result is a sharp drop in the lift coefficient, well below the value for the developed flow case, and a similar sharp increase in the drag coefficient, which assumes positive values in excess of the one found when no vortex interaction occurs. These effects continue after the vortex has passed over the trailing edge of the airfoil, with no evidence of a return to the conditions of the developed flow in the computed time interval. Finally, a comparison with the vorticity field obtained from the PIV measurement, presented in Figure 15, shows for the blade-vortex interaction the same behaviour just described from the LES computations, even if the vortex has a lower circulation.

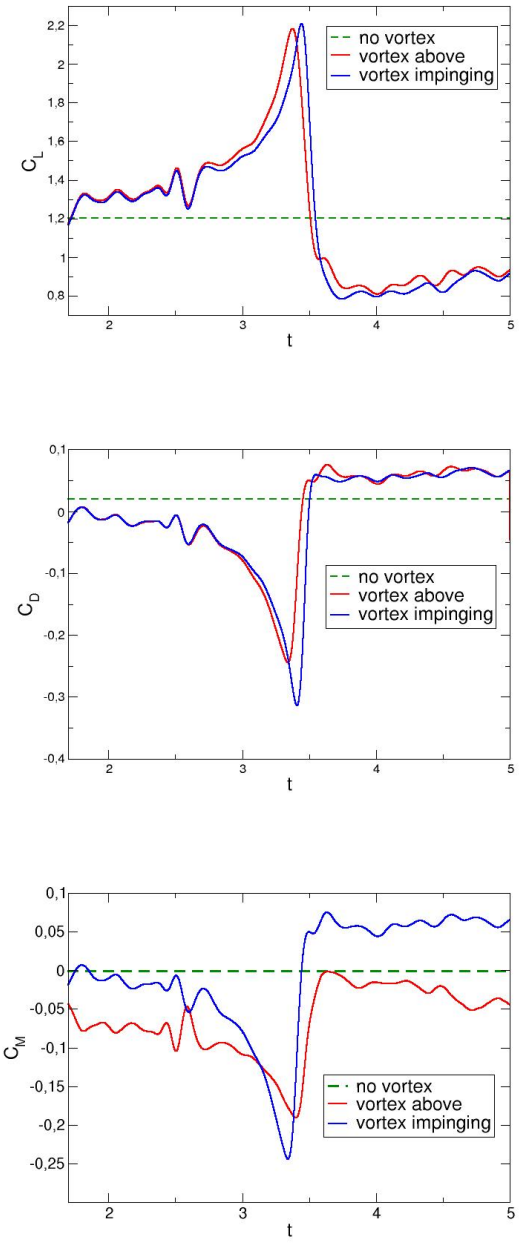

Figure 14: Time history of lift (top), drag (centre) and pitching moment (bottom) coefficients for the vortex interaction in both cases A and B, compared to the developed flow case (dashed line)

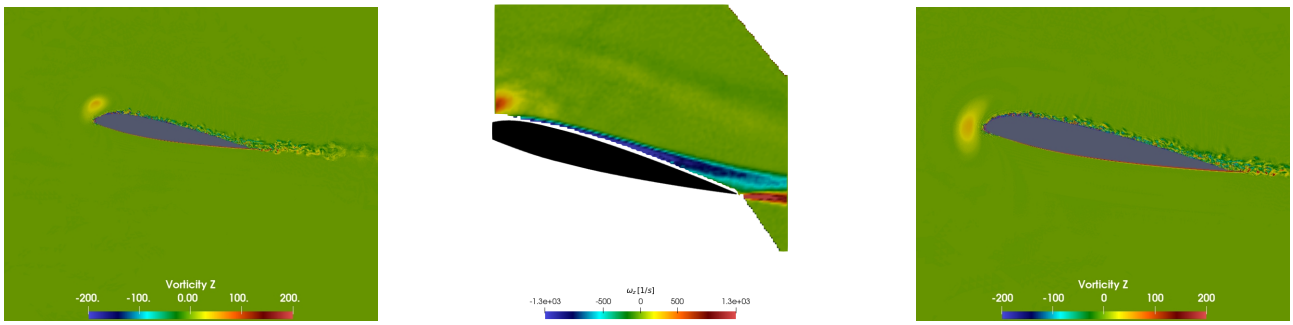

(a) $t = 3.4$

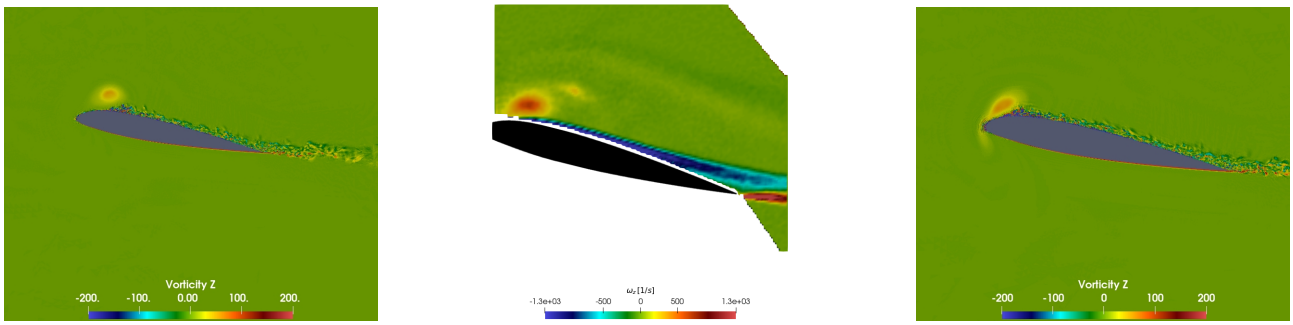

(b) $t = 3.5$

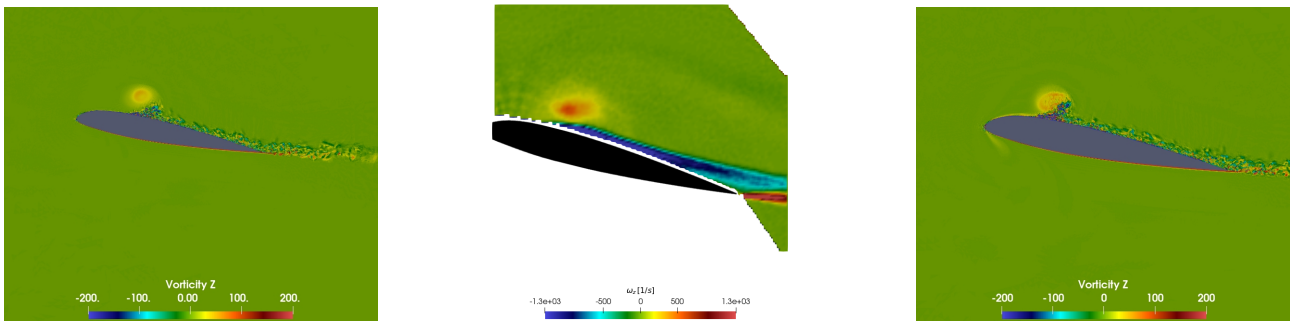

(c) $t = 3.6$

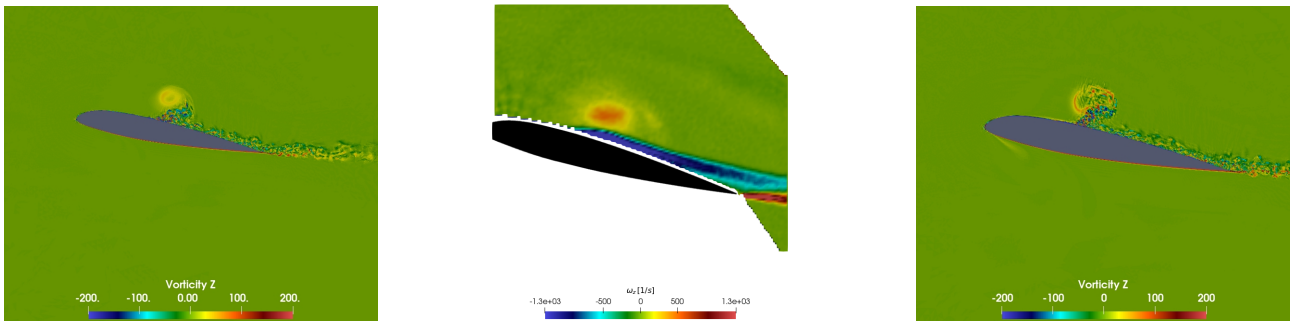

(d) $t = 3.7$

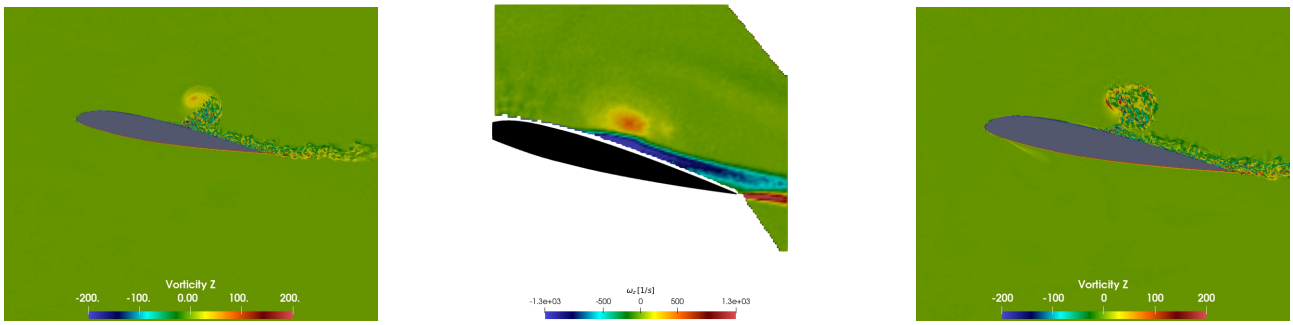

(e) $t = 3.8$

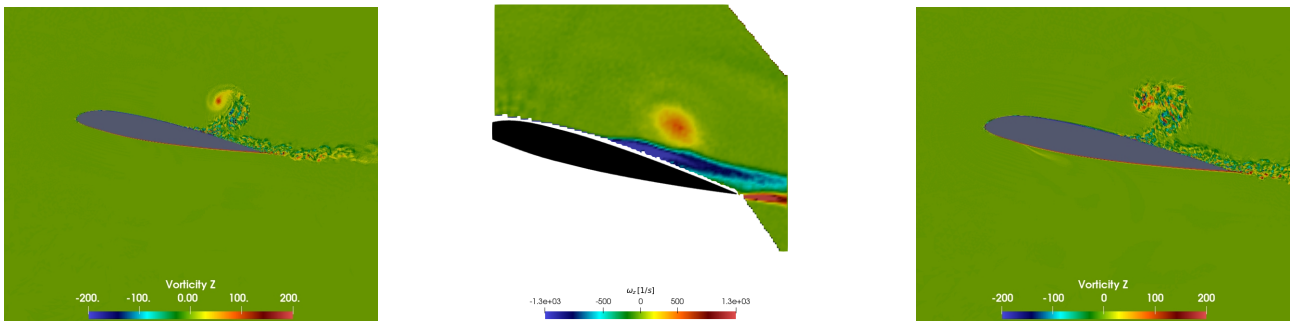

(f) $t = 3.9$

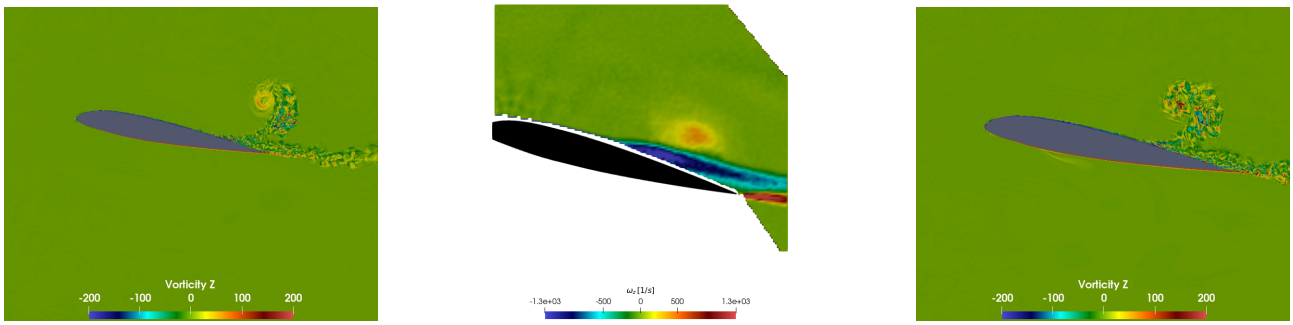

(g) $t = 4.0$

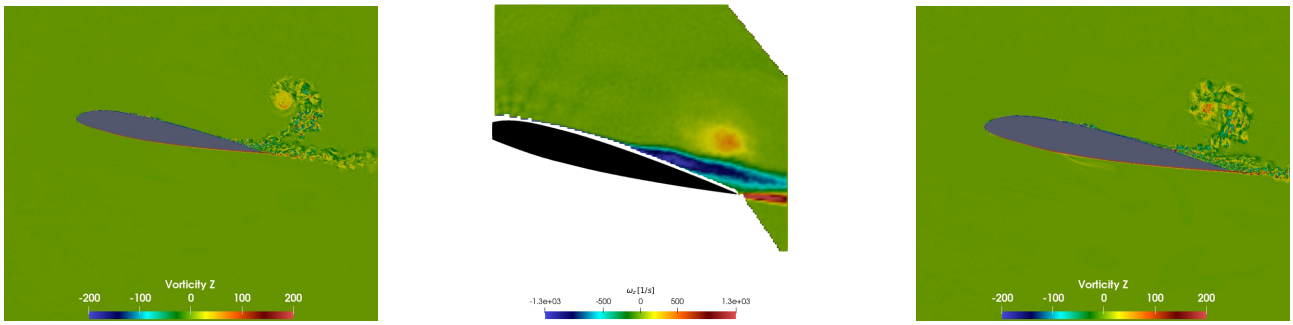

(h) $t = 4.1$

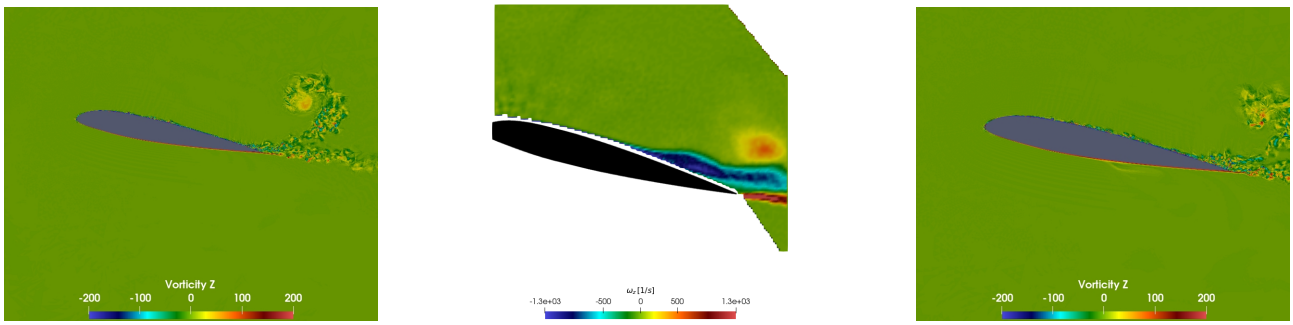

(i) $t = 4.3$

Figure 15: Time sequence of the vorticity field around the wing during vortex interaction, from PIV measurements (middle column) and LES computations (left column and right column representing vortex passing above and impinging on the leading edge, respectively).

5 CONCLUSIONS

In this work a dual approach, both experimental and numerical, to the study of parallel blade-vortex interaction has been successfully carried out. Large Eddy Simulation fitted with polynomial degree adaptivity has demonstrated to be a valid tool for the computation of such interactions, allowing to overcome the shortcomings of the experimental tests, such as the interfering presence of the vortex generator and a sub-optimal strength of the generated vortex.

Acknowledgments

The authors aknowledge that the results of this research have been achieved using the DECI resource *betzy* based in Norway at NTNU with support from the PRACE aisbl.

Copyright Statement

References

[1] Giovanni Droandi, Giuseppe Gibertini, and Alex Zanotti. Perpendicular blade–vortex-interaction over an oscillating airfoil in light dynamic stall. *Journal of Fluids and Structures*, 65:472–494, 2016.

[2] Giuseppe Gibertini, A Zanotti, and Andrea Colli. Dynamic stall inducted by blade vortex interaction in helicopter descending flight. In *45th European Rotorcraft Forum (ERF 2019)*, pages 168–172, 2019.

[3] François Richez. Analysis of dynamic stall mechanisms in helicopter rotor environment. *Journal of the American Helicopter Society*, 63(2):1–11, 2018.

[4] Alex Zanotti, Martino Ermacora, G Campanardi, and Giuseppe Gibertini. Stereo particle image velocimetry measurements of perpendicular blade–vortex interaction over an oscillating airfoil. *Experiments in Fluids*, 55(9):1–13, 2014.

[5] N M Chaderjian. Navier-stokes simulation of uh-60a rotor/wake interaction using adaptive mesh refinement. In *73rd American Helicopter Society International Annual Forum and Technology Display*, 2017.

[6] A Colli, G Gibertini, PU Krishna, V Marchesi, and A Zanotti. Parallel blade-vortex interaction on pitching airfoil. In *47th European Rotorcraft Forum (ERF 2021)*, pages 1–13, 2021.

[7] Antonella Abba and Andrea PC Bresciani. Large eddy simulation of parallel blade-vortex interaction on low reynolds airfoil. In *47th European Rotorcraft Forum (ERF 2021)*, pages 1–9, 2021.

[8] Andreas Goerttler, Johannes N Braukmann, Till Schwermer, Anthony D Gardner, and Markus Raffel. Tip-vortex investigation on a rotating and pitching rotor blade. *Journal of Aircraft*, 55(5):1792–1804, 2018.

[9] Marcel Ilie. A fully-coupled cfd/csd computational approach for aeroelastic studies of helicopter blade-vortex interaction. *Applied Mathematics and Computation*, 347:122–142, 2019.

[10] Antonella Abba, AC Cercignani, and Lorenzo Valdettaro. Analysis of subgrid scale models. *Computers & Mathematics with Applications*, 46(4):521–535, 2003.

[11] Antonella Abba, Luca Bonaventura, Michele Nini, and Marco Restelli. Dynamic models for large eddy simulation of compressible flows with a high order dg method. *Computers & Fluids*, 122:209–222, 2015.

[12] Matteo Tugnoli, Antonella Abbà, Luca Bonaventura, and Marco Restelli. A locally p-adaptive approach for large eddy simulation of compressible flows in a dg framework. *Journal of Computational Physics*, 349:33–58, 2017.

[13] Georgios H Vatistas. New model for intense self-similar vortices. *Journal of Propulsion and Power*, 14(4):462–469, 1998.

[14] Louis Rosenhead. The spread of vorticity in the wake behind a cylinder. *Proceedings of the Royal Society of London. Series A, Containing papers of a mathematical and physical character*, 127(806):590–612, 1930.